Structural Chemistry (2020) 31:485–505
https://doi.org/10.1007/s11224-019-01430-w

ORIGINAL RESEARCH

Structure of icosahedral quasicrystals within the multiple-cell approach

Alexey E. Madison[1] · Pavel A. Madison[2]

Received: 13 August 2019 / Accepted: 24 September 2019 / Published online: 7 January 2020

Abstract

The multiple-cell approach is discussed as an alternative to the higher-dimensional crystallographic description of icosahedral quasicrystals. Four types of quasi-unit cells fill the space without gaps and overlappings. Every cell in the whole tiling is decorated by specific atoms in a particular way and is associated with a triad: type, position, and orientation. The key features of the proposed approach are the subgroup/coset decomposition of icosahedral symmetry groups in accordance with the orbit-stabilizer theorem, a strict mathematical formalization of the substitution rules for all types of quasi-unit cells in the Socolar-Steinhardt tiling, formalization of the recursive inflation/deflation rules, and the eigenvalue-eigenvector analysis of corresponding substitution matrices. The similar approach can be applied to almost all types of quasicrystals.

Keywords Quasicrystals · Icosahedral symmetry · Substitution tiling · Group theory

Introduction

Discovery of quasicrystals by Shechtman [1] is now considered as one of the milestones in the development of modern crystallography. Shortly before that, Mackay [2] simulated the diffraction pattern of the Penrose tiling and made evident its 5-fold symmetry and the presence of sharp diffraction peaks. Steinhardt et al. [3, 4] provided the first theoretical explanation of infinite icosahedral packings and showed that a long-range orientational order with no translational periodicity can also exist in three dimensions just in the same way as the Penrose tiling represents such an example in two dimensions. These important breakthroughs led to paradigm shift in our understanding of the nature of chemical structures. Under the term "crystal" we now understand any solid having an essentially discrete diffraction pattern. According to the more strict mathematical definition, an aperiodic crystal is a distribution of discrete point masses that has a pure point Fourier transform. The ordinary crystals are periodic distributions with periodic spectra, while quasicrystals are usually self-similar distributions with self-similar spectra.

The atomic structure of quasicrystals is usually described within the superspace formalism by using the cut-and-project construction [5–15]. Another approach is based on the concept of quasi-unit cells [16–22] or overlapping clusters [23–27]. Additional information on the atomic structure, spatial arrangement, and linkage of icosahedral shell clusters in crystalline approximants provides a good starting point for structure analysis of quasicrystals [28–31]. Different approaches emphasize different aspects of quasicrystals, thus mutually reinforcing each other. Taken separately, none of these methods guarantees that the most accurate and comprehensive understanding of the nature of long-range aperiodic order is gained [32]. For the historical aspects of the discovery itself, development and cross-fertilization of related ideas and concepts, see [33–35].

Recently, we proposed an approach based on the recurrent construction of the Socolar-Steinhardt zonohedral tiling with subsequent decoration of quasi-unit cells with specific atoms [36–39]. We therefore divided the whole problem into two separate steps: filling the space with polyhedra and filling the polyhedra with atoms. The major advantage of the multiple-cell approach is that the most problems can seemingly be solved without leaving the real physical 3D space.

✉ Alexey E. Madison
alex_madison@mail.ru

[1] Center for Advanced Studies, Peter the Great St. Petersburg Polytechnic University, ul. Polytechnicheskaya 29, Saint Petersburg, 195251, Russia

[2] Department of Micro- and Nanoelectronics, St. Petersburg Electrotechnical University 'LETI', ul. Professora Popova 5, Saint Petersburg, 197376, Russia

Four types of golden zonohedra serve as quasi-unit cells: the prolate rhombohedron, the rhombic dodecahedron, the rhombic icosahedron, and the rhombic triacontahedron. They fill the space without gaps and overlappings. Every cell in the whole tiling is decorated by specific atoms in a particular way and is associated with a triad: type, position and orientation. Only the full set of quasi-unit cells ensures packing homogeneity. Periodic crystals can be constructed by stacking identical unit cells face-to-face in perfect alignment in three dimensions. Similarly, icosahedral quasicrystals can be defined as packings of identical quasi-unit cells, with a few minor differences: (i) there are four cell types instead of a single one and (ii) a special hierarchical packing algorithm is used instead of lattice translations.

Detailed description of the whole algorithm is provided below. The key steps are the following:

- A group-theoretical analysis of icosahedral symmetry paying special attention to the subgroup/coset decomposition of both $I\,(235)$ and $I_h\,(m\overline{3}5)$ icosahedral groups and to the orbit-stabilizer theorem.
- A strict mathematical formalization of the substitution rules for all types of quasi-unit cells in the Socolar-Steinhardt tiling.
- Formalization of the space-filling algorithm based on recursive inflation/deflation rules.
- Enumeration of general and special positions inside the cells and on their surfaces bearing in mind their local symmetry and some additional restrictions.
- Calculation of the packing density and compound stoichiometry based on the eigenvalue-eigenvector analysis of the substitution matrix.
- Averaging of the structure factors over quasi-unit cells based on a procedure similar to the Perron projection.
- Confirmation of the validity of the approach through the comparison of characteristic clusters and their spatial arrangement with those obtained by the cut-and-project method.

Group-theoretical analysis

The subgroup/coset decomposition plays a key role in understanding both the space-filling and decoration algorithms. The elements of the stabilizer subgroups send quasi-unit cells to themselves, hence define the atomic cell decorations. Otherwise, all the other group elements generate the orbits of quasi-unit cells and, therefore, describe the mutual cell arrangement.

Icosahedral symmetry can be described by the two groups: I and I_h, respectively. The group I consists of 60 orientation-preserving rotations, whereas I_h in addition includes mirror reflections and improper rotations. Up to now it was generally believed that I_h is the proper symmetry group of all the icosahedral quasicrystals, simply because all the structure refinements were made under such assumption with the varying degrees of success. On the other hand, existence of non-centrosymmetric icosahedral quasicrystals has been neither proved nor disproved so far.

The icosahedral symmetry has been extensively treated in literature [40–44]. Unfortunately, various authors use different notations and enumerate the group elements in different ways. For instance, the group elements may be interpreted either as rotations and reflections of an icosahedron or as cyclic permutations depending on the context. If the main concern is the structure of icosahedral viruses, the numbering of rotation matrices inherits specific numbering scheme of capsomers adopted in the description of viral capsids [45, 46]. On the contrary, enumeration according to the conjugacy classes is commonly adopted in solid-state physics [47]. The choice of the default (standard) orientation of an icosahedron also differs from paper to paper. That is why the existing multiplication tables, rotation matrices, and coset decompositions of the corresponding group-subgroup pairs cannot be used directly. We followed Litvin [41] in choosing the orientation of an icosahedron and the vertex numbering scheme (Fig. 1).

The group generators are given in Table 1. In this table, $u = (\sqrt{5}+1)/4 = \tau/2$, $v = (\sqrt{5}-1)/4 = (\tau-1)/2$, where $\tau = (1+\sqrt{5})/2$ is the golden mean. The first three elements generate the group I. The group I_h may be obtained by adding the inversion element to I.

Any group element may be unambiguously defined in terms of cyclic permutations of numbered icosahedron vertices. Both Schoenflies and Hermann-Mauguin notation may be used to identify the symmetry transformations.

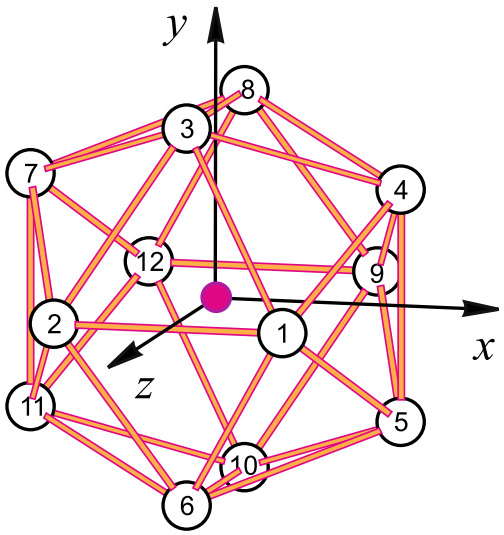

Fig. 1 Numbering of the vertices of an icosahedron

Additional numbers in parentheses (or additional indices as subscripts) specify the corresponding vertex permutations. Strictly speaking, the subscript indices in Hermann-Mauguin notation are reserved to denote the screw axes. Since screw axes are incompatible with icosahedral symmetry, we found that it possible to use subscripts for specifying the vertex numbers in hope that this will not lead to the confusion of notation. For example, the cycle (1)(2 6 5 4 3)(7 11 10 9 8)(12) corresponds to the counterclockwise rotation around the 5-fold axis passing through the vertex 1. It is denoted as 5_1. The cycle (1 3 2)(4 7 6)(5 8 11)(9 12 10) corresponds to the counterclockwise rotation around the 3-fold axis normal to the triangle $\triangle 123$. We denote it as 3_{132}, and so on. As usual, we assume that counterclockwise rotations are positive when looking at the icosahedron from the outside. All group elements are numbered according to conjugacy classes:

$$
I_h = \left\{ \begin{array}{ll}
E & = \{e\}, \\
12C_5 & = \{5_1, 5_2, 5_3, 5_4, 5_5, 5_6, 5_1^4, 5_2^4, 5_3^4, 5_4^4, 5_5^4, 5_6^4\}, \\
12C_5^2 & = \{5_1^2, 5_2^2, 5_3^2, 5_4^2, 5_5^2, 5_6^2, 5_1^3, 5_2^3, 5_3^3, 5_4^3, 5_5^3, 5_6^3\}, \\
20C_3 & = \{3_{132}, 3_{143}, 3_{154}, 3_{165}, 3_{126}, 3_{237}, 3_{387}, 3_{348}, 3_{498}, 3_{459}, \\
 & \quad 3_{132}^2, 3_{143}^2, 3_{154}^2, 3_{165}^2, 3_{126}^2, 3_{237}^2, 3_{387}^2, 3_{348}^2, 3_{498}^2, 3_{459}^2\}, \\
15C_2 & = \{2_{12}, 2_{13}, 2_{14}, 2_{15}, 2_{16}, 2_{23}, 2_{34}, 2_{45}, 2_{56}, 2_{26}, 2_{27}, 2_{37}, 2_{38}, 2_{48}, 2_{49}\}, \\
C_i & = \{\bar{1}\}, \\
12S_{10}^3 & = \{\bar{5}_1, \bar{5}_2, \bar{5}_3, \bar{5}_4, \bar{5}_5, \bar{5}_6, \bar{5}_1^9, \bar{5}_2^9, \bar{5}_3^9, \bar{5}_4^9, \bar{5}_5^9, \bar{5}_6^9\}, \\
12S_{10} & = \{\bar{5}_1^7, \bar{5}_2^7, \bar{5}_3^7, \bar{5}_4^7, \bar{5}_5^7, \bar{5}_6^7, \bar{5}_1^3, \bar{5}_2^3, \bar{5}_3^3, \bar{5}_4^3, \bar{5}_5^3, \bar{5}_6^3\}, \\
20S_6 & = \{\bar{3}_{132}, \bar{3}_{143}, \bar{3}_{154}, \bar{3}_{165}, \bar{3}_{126}, \bar{3}_{237}, \bar{3}_{387}, \bar{3}_{348}, \bar{3}_{498}, \bar{3}_{459}, \\
 & \quad \bar{3}_{132}^5, \bar{3}_{143}^5, \bar{3}_{154}^5, \bar{3}_{165}^5, \bar{3}_{126}^5, \bar{3}_{237}^5, \bar{3}_{387}^5, \bar{3}_{348}^5, \bar{3}_{498}^5, \bar{3}_{459}^5\}, \\
15\sigma & = \{m_{38}, m_{49}, m_{37}, m_{48}, m_{27}, m_{15}, m_{16}, m_{12}, m_{13}, m_{14}, m_{34}, m_{26}, m_{45}, m_{23}, m_{56}\}
\end{array} \right\} = I; \tag{1}
$$

As will be shown below, we have to know the multiplication tables of both icosahedral groups. The easiest way is to use the Wolfram Mathematica® Combinatorica package. First, we use the standard procedure to generate the permutation group with a given set of generators. Then, we put the cycles into one-to-one correspondence with their "crystallographic names" (stored as string variables) and with the rotation matrices. Next, we look for the required permutation and apply it to the set of elements to put the elements in the right order. Finally, we write down the full list of elements and compute the multiplication tables.

The full set of quasi-unit cells consists of four golden zonohedra: the rhombic triacontahedron, the rhombic icosahedron, the rhombic dodecahedron, and the prolate golden rhombohedron (Fig. 2). Marking of the triacontahedron vertices inherits the numbering scheme for the icosahedron. We draw the reader's attention to the positions of the local cell origins. Any quasi-unit cell can be inscribed within a triacontahedron, so that the local origins of all cells coincide.

Four types of golden zonohedra are to be inflated by the scaling factor of τ^3 and deflated back to the original size [36–39]. In the whole packing, quasi-unit cells can appear in different orientations, which nevertheless comply with the global icosahedral symmetry. Therefore, for every quasi-unit cell, we need to single out one of the possible orientations, which, hereinafter, we refer to as the standard or default orientation of specific quasi-unit cell. Purely for the convenience's sake, it was preferable that the main symmetry axes lay in the xy-plane whenever possible (see Fig. 2).

Consider one of the quasi-unit cells and apply the group action to it. A special subgroup, the elements of which send the cell to itself, is called its stabilizer. The remaining elements generate the orbit of the cell in accordance with the orbit-stabilizer theorem. Figure 3 shows the orbits of all quasi-unit cells under the action of group I. Here we pay more attention to the group I, as the action of I_h is quite similar and generates the same orbits with the only difference that twice as much elements make up the corresponding left cosets and stabilizers.

The stabilizer of the rhombohedron consists of 3 symmetry transformations: the identity element and the 3-fold axis with its reverse. Therefore, the corresponding orbit consists of 20 differently oriented rhombohedra. The stabilizer of the rhombic dodecahedron has 2 elements: the identity and the 2-fold axis. It can thus be oriented in exactly 30 different ways. The stabilizer of the rhombic icosahedron has 5 elements: the identity and the 5-fold axis with its powers. It can be oriented in 12 ways. The rhombic triacontahedron has the trivial stabilizer: the group I itself. Its orbit has the length of 1. There are no additional ways

Table 1 The generators of the icosahedral groups I and I_h

#	Schoenflies notation	Hermann-Mauguin notation	Cyclic permutation	Rotation matrix
2	$C_5(1)$	5_1	(1)(2 6 5 4 3)(7 11 10 9 8)(12)	$\begin{pmatrix} 1/2 & -u & v \\ u & v & -1/2 \\ v & 1/2 & u \end{pmatrix}$
26	$C_3(132)$	3_{132}	(1 3 2)(4 7 6)(5 8 11)(9 12 10)	$\begin{pmatrix} -1/2 & -u & v \\ u & -v & 1/2 \\ -v & 1/2 & u \end{pmatrix}$
46	$C_2(12)$	2_{12}	(1 2)(3 6)(4 11)(5 7)(8 10)(9 12)	$\begin{pmatrix} -1 & 0 & 0 \\ 0 & -1 & 0 \\ 0 & 0 & 1 \end{pmatrix}$
61	C_i	$\bar{1}$	(1 12)(2 9)(3 10)(4 11)(5 7)(6 8)	$\begin{pmatrix} -1 & 0 & 0 \\ 0 & -1 & 0 \\ 0 & 0 & -1 \end{pmatrix}$

to orient it in space. According to the Cauchy-Frobenius lemma known also as the orbit counting theorem: $3 \cdot 20 = 2 \cdot 30 = 5 \cdot 12 = 1 \cdot 60 = 60$.

Now we can turn to the description of the packing. We said that every cell can be associated with a triad: type, position, and orientation. The cell type can be interpreted as an integer in the range from 1 (rhombohedron) to 4 (triacontahedron). The position is defined as the Cartesian coordinates of the specific cell's local origin in the global coordinate system. In the "Substitution rules" section, we demonstrate that the position of any cell in an icosahedral quasicrystal, regardless of its type and orientation, can always be described by the set of 6 integers. Finally, the orientation of any cell can be associated with the first group element of the corresponding coset. In other words, it can be defined as an integer in the range from 1 to 60. For the group I_h the first (representative) element of the coset is also within the range of 1 to 60.

To generate the whole packing, we use consecutive inflations and deflations. As a result, some of subcells can

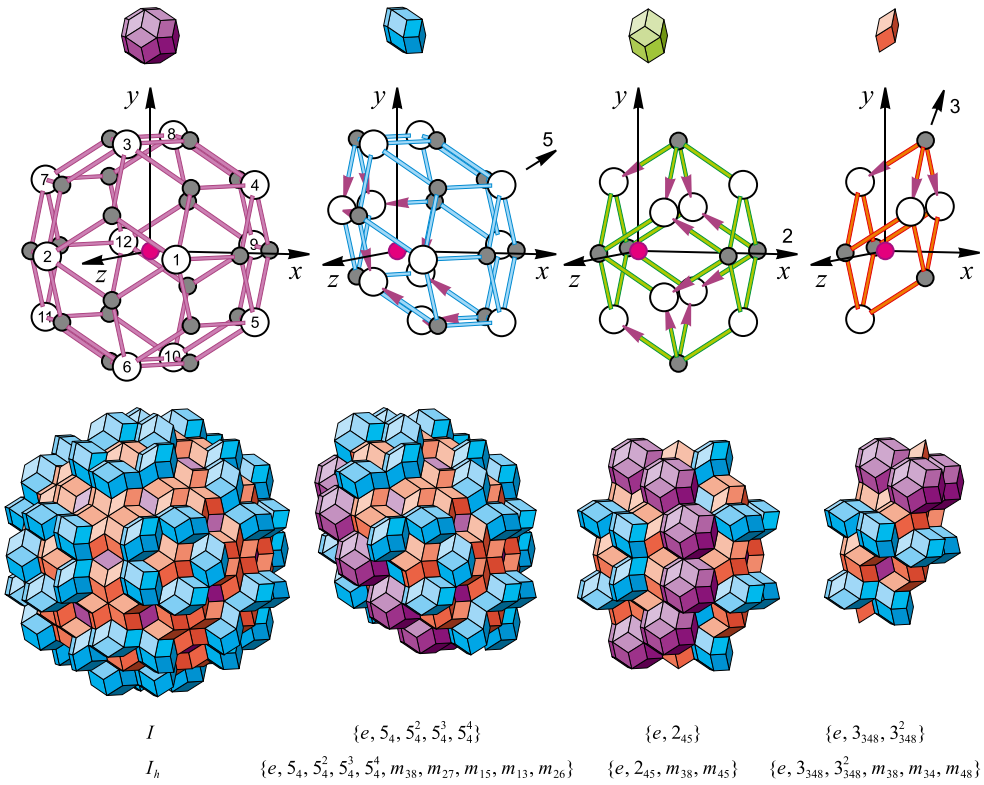

Fig. 2 Default orientations of quasi-unit cells. Four types of golden zonohedra are inflated by the scaling factor of τ^3 and deflated back to the original size. Stabilizer subgroups are written down below the cells to which they relate for both I and I_h groups, respectively

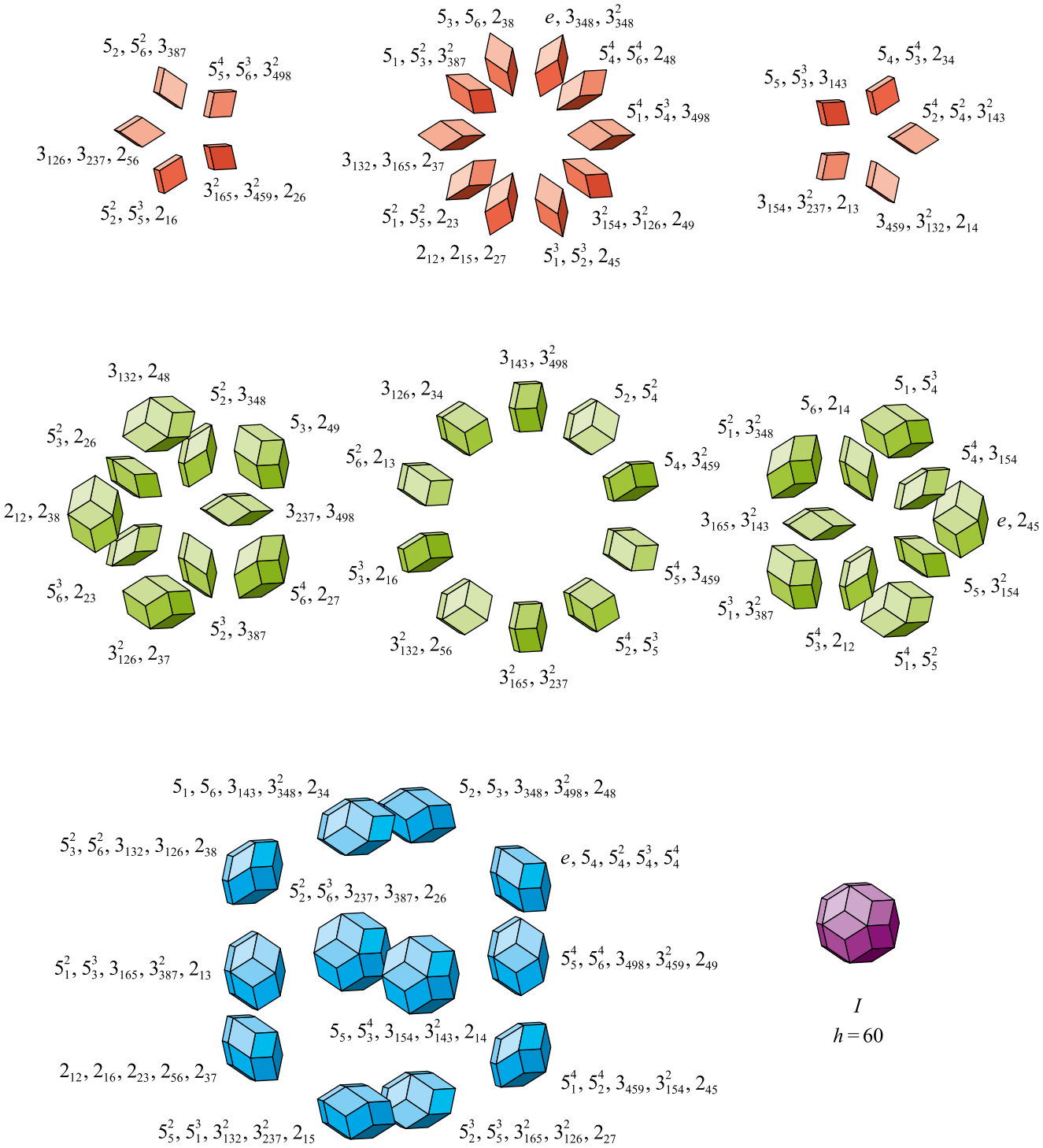

Fig. 3 Orbits of quasi-unit cells under the action of group I. Symmetry elements next to the differently oriented quasi-unit cells represent the left cosets of the corresponding stabilizer subgroups

be shared by two or more adjacent supercells [36, 37]. To avoid the multiple counting, we can delete the redundant cells and redirect the links to the already existing ones. However, when performing calculations with substitution matrices, it might be more convenient to assign weighting factors to shared cells (sharing factors). We discuss the sharing factors for cells and atoms in the "Substitution rules" and "Filling the quasi-unit cells with atoms" sections, respectively.

Substitution rules

The zonohedral tiling has been invented by Socolar and Steinhardt [4]. Ogawa pointed out that, in the most general case, the linear scaling factor of a 3D icosahedral tiling should be equal to τ^3 [48]. The substitution rules were derived thirty years later [36, 37].

The set of four golden zonohedra is not the only way to construct an icosahedral packing. However, the ABCK Danzer tiling [49] has the inflation factor of τ (see, e.g., Ch. 6 in [50]), which is not in line with the experimental data [12]. The tiling by prolate and oblate rhombohedra does not preserve the exact icosahedral symmetry and is thus applicable only on average. That is why Socolar and Steinhardt made a definitive conclusion that the zonohedral tiling "must be accepted as one of the necessary subtleties of the 3D icosahedral construction" [4]. Curiously, the complete set of four non-overlapping zonohedra has never been used to interpret the experimental data so far.

At the first glance, the substitution rules [36, 37] seem to be rather cumbersome. For example, 533 different polyhedra should be taken into account when deflating the triacontahedron. It might even seem that such a huge number of subcells would make the rules almost worthless—far from it. In fact, the rules are very natural and simple, because only 12 of 533 polyhedra are independent (Fig. 4). Allow us to explain the basic principles that govern the packing geometry.

First, we redefine the equivalence relations between corresponding quasi-lattice sites. In a generalized sense, there are only three types of inequivalent sites in the Socolar-Steinhardt tiling: A, B, and C. Consider a triacontahedron. It has 12 icosahedral and 20 dodecahedral vertices, which we refer to as the A and B types, respectively. As a result of inflations and deflations, any A-type vertex turns into a star of rhombohedra surrounded by 12 rhombic icosahedra, while any B-type vertex turns into a similar star but surrounded by 12 rhombic triacontahedra. All vertices in the whole tiling are equivalent to either A or B type in this sense. The center of a triacontahedron, which we refer to as the C-type site, transforms into a triacontahedron again. More generally, a local origin of any quasi-unit cell turns into a triacontahedron. None of the self-similarity operations can change the vertex type. Therefore, if we consider an ABC triangle in a triacontahedron and inflate it with a linear scaling factor of τ^3, its vertices become occupied by two stars and a triacontahedron, respectively (see Fig. 4).

Second, the icosahedral symmetry should not be destroyed after deflations. Therefore, only those cells and

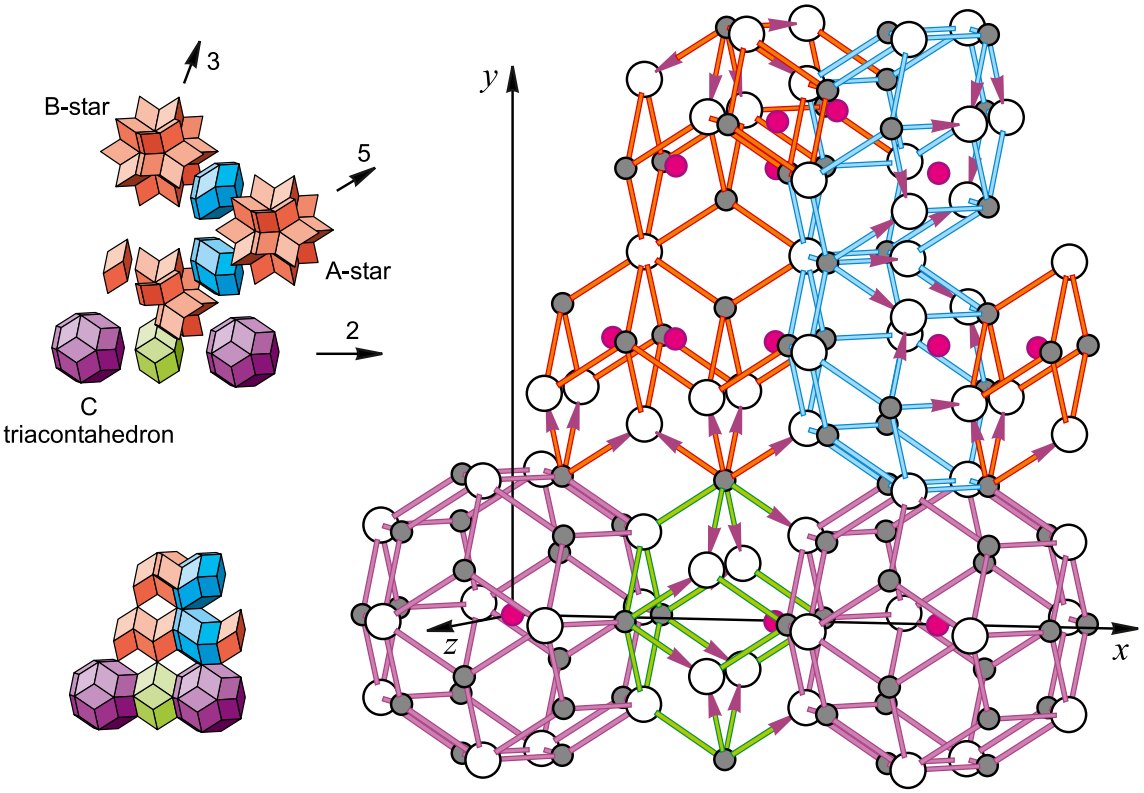

Fig. 4 Substitution rules for the triacontahedron: the ABC triangle and 13 independent polyhedra (for the group I). This number decreases to only 12 independent polyhedra for the group I_h. Enlarged cells illustrate the compliance of the deflation with matching rules

clusters, which in themselves obey the 2-fold symmetry, may be stacked along the 2-fold axis. Only those cells, which in themselves obey the 3-fold symmetry, may be stacked along the 3-fold axis. Only those cells and clusters, which in themselves obey the 5-fold symmetry, may be stacked along the 5-fold axis. This means that only triacontahedra and rhombic dodecahedra may alternate along the 2-fold axis when deflating the triacontahedron. Only triacontahedra and rhombohedra may alternate along the 3-fold axis. Only triacontahedra and rhombic icosahedra together with clusters of five rhombohedra or five rhombic dodecahedra arranged around a common edge may alternate along the 5-fold axis.

Third, inflations and deflations must not be inconsistent with the higher-dimensional approach. We emphasize again and again that both approaches are not contradictory. Surely, the central part of the tiling obtained by substitutions [39] coincides with that one obtained by projection [4], the types of faces and the local matching rules complies with those described in terms of Ammann plane decorations, and so forth. As to the packing rules, we would rather give a quote [4], "The Ammann planes distinguish only three different types of rhombic faces on surfaces of the unit cells. Two adjacent cells must be joined along faces with identical markings and orientations."

To summarize, the Socolar-Steinhardt tiling is formed by four types of quasi-unit cells. Three locally isomorphic packings with exact icosahedral point symmetry can be built by the same rules. According to this, there exist only three types of special sites in the packing (A, B, and C). There are two types of edges (E_1 and E_2; we mark the second type edges with arrows) and three types of faces (F_1, F_2, and F_3). For more details, see [36–38].

When all these reasonings are taken into account, the solution becomes almost evident (Fig. 4). We encourage the reader to compare these simple rules and the cell packing order with those based on the incomplete set of zonohedra (see Fig. 3 in [11]). The deflation rules can be formally written in exactly the same way as those for the cell packing procedure—by specifying the types, positions, and orientations of subcells. Independent subcells that define the decomposition rule of a triacontahedron are listed in Table 2.

We followed Levine and Steinhardt [3] in choosing the scale, so that the prolate rhombohedron would have unit volume. The volumes of basic zonohedra are therefore in the ratio of $1 : 2\tau : 5\tau : 10\tau$. The two initial triacontahedron vertices have coordinates $A(1+\tau, \tau, 0)$ and $B(1+\tau, 0, 1)$; all the others can be determined by applying the group action to these two initial points. Any edge in the packing can be associated with one of the 12 vectors, which in turn can be obtained through rotating an initial vector $(\tau, 1, 0)$. The position of any cell, as well as the position of any vertex in the entire tiling, can be expressed as a linear combination of 6 basic vectors with integer coordinates $(i + j\tau, k + l\tau, m + n\tau)$, as though two incommensurate cubic lattices would coexist simultaneously—one with lattice constant a and the other with τa, respectively. Indeed, this statement holds true for the initial triacontahedron vertices. The same holds true for any of differently oriented edge vectors. Therefore, the exact position of any of the quasi-lattice sites may be defined by six integers.

In Table 2, most of the subcells have the sharing factors equal to 1. This means that corresponding subcells come into the supercell as a whole. For the last three subcells, the sharing factors are fractions less than 1. The corresponding

Table 2 Deflation rule for the triacontahedron

Type	Position	Orientation		Sharing	Multiplicity
		#	Element	factor	factor
4	$(0, 0, 0)$	1	e	1	1
2	$(2+\tau, 0, 0)$	46	2_{12}	1	30
4	$(2+4\tau, 0, 0)$	1	e	1	30
1	$(2, 2+2\tau, 0)$	46	2_{12}	1	20
1	$(2\tau, 2+2\tau, 0)$	20	5_1^3	1	60
1	$(2+2\tau, 2+2\tau, 0)$	46	2_{12}	1	60
3	$(2+4\tau, 2+2\tau, 0)$	46	2_{12}	1	12
1	$(4+4\tau, 2+2\tau, 0)$	46	2_{12}	1	60
1	$(2\tau, 2+4\tau, 0)$	1	e	1	20
1	$(2+2\tau, 2+4\tau, 0)$	4	5_3	1	60
3	$(2+4\tau, 2+4\tau, 0)$	16	5_3^2	2/5	60
1	$(1+3\tau, 3+4\tau, \tau)$	3	5_2	1/2	60
1	$(1+3\tau, 3+4\tau, -\tau)$	2	5_1	1/2	60

subcells are shared by two or more adjacent supercells. In particular, only 2/5th of the rhombic icosahedron and only halves of the last two rhombohedra fall within the inflated triacontahedron under consideration.

The last two rows can be merged when considering the symmetry group I_h. It is then sufficient to consider only one of these two rhombohedra with a multiplicity factor of 120. Thus, the minimal set of independent subcells consists of only 12 zonohedra. All other subcells in the decomposition can be derived simply by applying group action to the above 12 independent ones. All we really need is the rotation matrices and the group multiplication table. It is easy to see that the sum of all entries in the last column is 533, i.e., the total number of cells in the decomposition.

It would be ineffective to verify every time to which of the cosets belongs the result of the group multiplication. Fortunate, we have no need for doing so. We prepare four copies of the group multiplication table (one for each cell type) and then go through all entries and replace them by the first elements of the corresponding cosets (see Fig. 3). When using such an array of four "modified" multiplication tables in order to determine the orientation of specific cell as a result of rotation, one immediately gets the first element of the coset.

When the decomposition rule for the triacontahedron is obtained, it is not hard to derive the rules for all the other cell types simply by analogy [36, 37]. The only complication appears when considering how the shared subcells are oriented in space. In this case, we just have to bear in mind that the edges must connect the vertices of different types only: A and B.

After the deflation rules for smaller cells in their default orientation are derived, we apply the group action to them. We rotate the inflated cells, with all the subcells inside, about their local origins by representative elements of the cosets. It is suitable to store the deflation rules as a special array. Its first 20 entries contain the deflation rules for rhombohedra, its next 30 entries contain the rules for rhombic dodecahedra, and so forth, so that totally there are $20 + 30 + 12 + 1 = 63$ entries for all cells in all possible orientations.

Filling the space with quasi-unit cells

In order to generate the Socolar-Steinhardt tiling, we have to apply an iterative algorithm to initial cell/cells. We would like to give another quote of Socolar and Steinhardt [4], "There are three complete packings with a (single) center of icosahedral point symmetry. One of these has a triacontahedron at its center, the next shell being composed of thirty dodecahedra. The other two have a star at their centers, one having twelve icosahedra as the next shell, the other having twelve triacontrahedra." All the three fundamental icosahedral packings can be obtained by applying the same inflation/deflation rules. The result depends only on where the origin is set (Fig. 5). The corresponding initial cells are listed in Table 3.

The structure of an icosahedral quasicrystal is defined recursively as a collection of quasi-unit cells. In other words, the data storage is organized as a rooted tree. We start with a fictitious root node that points to the common ancestor. For example, a triacontahedron represents a single parent when considering the packing centered at the C-type site. It becomes a common ancestor for all cells in the entire packing. When considering the A- and B-centered packings, the stars of 20 differently oriented rhombohedra define the initial sets of parent cells.

Allow us to describe the C-type tree in more detail. An initial triacontahedron has 533 children, each of which has its own descendants according to the deflation rule of the specific cell, and so forth. If we do not want to deal with weighting factors and wish to avoid the duplicate counting, we should delete the redundant shared cells and redirect the appearing dangling links to the existing cells. Note that, strictly speaking, the resulting graph will be no longer a rooted tree after resolving the duplicate counting.

The cell generation algorithm is surprisingly simple (see Fig. 6 for an illustrative example):

$$\begin{cases} \mathbf{R}_k = \tau^3 \mathbf{R}_i + g_i \mathbf{R}_j \\ g_k = g_i g_j \end{cases} \tag{2}$$

Here, $\mathbf{R}_i$ and g_i denote the position and orientation of an existing cell (parent), $\mathbf{R}_j$ and g_j denote the position and orientation of the cell being generated (child) in the standard deflation scheme of the parent, and $\mathbf{R}_k$ and g_k denote the position and orientation of the child cell in the entire tiling, respectively.

If we know the deflation rules for the parent cell in its default orientation, we always can rotate it, with all the other stuff inside, to get the deflation scheme of the rotated cell. We have merely to multiplicate the positions and orientations of subcells with corresponding group element. When the substitution rules for the rotated cells are derived, the remainder of the tree generation procedure becomes quite evident.

We reiterate that, when determining the cell orientations, we do not perform the actual matrix multiplication. To get the result, we take one of four "modified" multiplication tables and find the number of the required group element at the intersection of the corresponding row and column.

One more advantage of the algorithm should be noted. Once generated, the cell positions do not change anymore. The packing grows step by step, shell by shell, but adding new cells does not affect the existing ones.

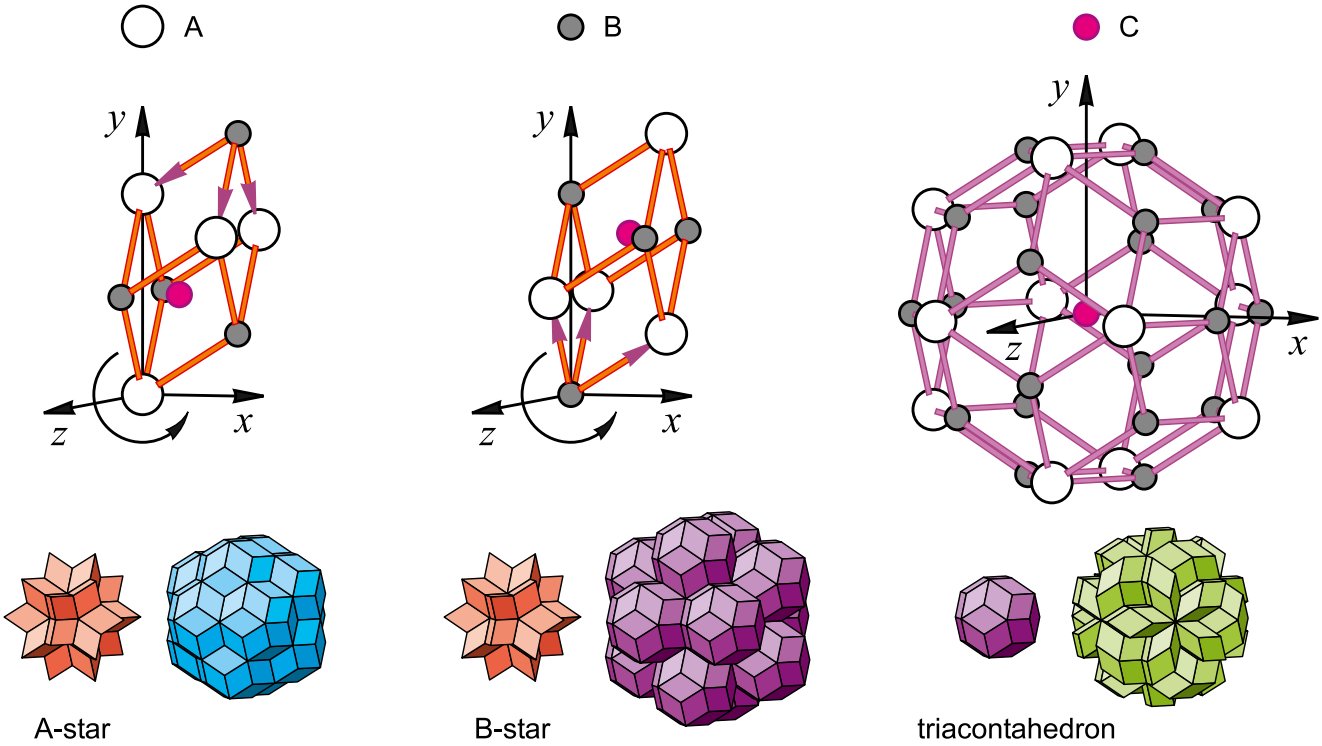

Fig. 5 Initialization of the space-filling algorithm. Three locally isomorphic packings with exact icosahedral point symmetry can be built by applying the same inflation/deflation rules depending on where the origin is set. The innermost shells of the perfect icosahedral packings can be formed either by a star of 20 rhombohedra surrounded by 12 rhombic icosahedra, by a star of 20 rhombohedra surrounded by 12 triacontrahedra, or by a triacontahedron surrounded by 30 rhombic dodecahedra

Filling the quasi-unit cells with atoms

There is a widespread perception that "the atomic decoration of the tiles may not be uniform all over the tiling" [51] and that "quasicrystals cannot be defined as packings of identical unit cells" [23]. Our primary goal is to show that the uniform decoration of quasi-unit cells is, nevertheless, possible. We are also going to demonstrate how the groups I and I_h can be separated from each other through the appropriate cell decoration.

We specify the sets of special and general positions, similar to Wyckoff positions in conventional periodic crystals: inside the cells, on the faces, on the edges, and at the vertices (see Table 4). The valid decoration scheme must be consistent with the cell symmetries, local matching rules, and some additional restrictions caused by the local isomorphism of the tiling [39].

First, as we have already mentioned, the symmetry group of each cell is the subgroup of the given group. Distribution of atoms inside the cells must obey the corresponding stabilizer subgroup. For example, considering the decoration of zonohedra by the Ammann planes, Socolar and Steinhardt showed that the decorated rhombic dodecahedron has only two planes of reflection symmetry. "The dodecahedron itself has a third mirror plane, but this symmetry is not respected by the Ammann plane decoration" [4]. More generally, at least three of four quasi-unit cells are not centrosymmetric, even for the group I_h.

It is quite surprisingly, but the vast majority of structure refinements have been made up to now under an assumption

Table 3 Initialization of the space-filling algorithm

Origin	Type	Position	Orientation		Multiplicity
			#	Element	factor
A	1	$(-1+\tau, \tau, 0)$	1	e	20
B	1	$(1, 1+\tau, 0)$	46	2_{12}	20
C	4	$(0, 0, 0)$	1	e	1

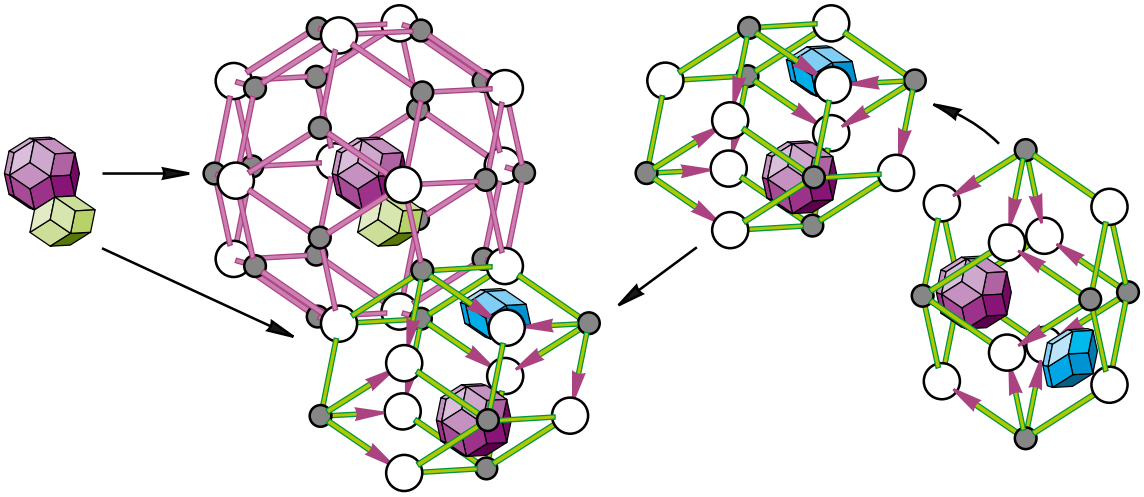

Fig. 6 Illustration of the recursive space-filling algorithm. The initial triacontahedron is a common ancestor for all cells in the tiling. In the current step, the rhombic dodecahedron (the small green cell) is considered as an example of the parent cell. It has been generated in the previous step by applying the inflation/deflation rules to a triacontahedron. Its position and orientation are $\mathbf{R}_i$ and g_i, respectively. As a result of inflation, the origin of the inflated parent cell shifts to $\tau^3\mathbf{R}_i$. The rhombic icosahedron (the small blue cell) is one of those cells, which are to be generated in the current step. It is a child cell of the rhombic dodecahedron and a descendant of the initial triacontahedron. Its position and orientation in the standard deflation scheme of the rhombic dodecahedron (right) are $\mathbf{R}_j$ and g_j, respectively. The group element g_i acts on the rhombic dodecahedron and rotates it as a whole with all the other stuff inside. The position and orientation of the child cell become $g_i\mathbf{R}_j$ and $g_i g_j$, respectively. Finally, the position and orientation of the newly generated cell with respect to the global coordinate system become $\tau^3\mathbf{R}_i + g_i\mathbf{R}_j$ and $g_i g_j$, respectively

Table 4 Inequivalent positions in icosahedral quasicrystals

Position	Coordinates	Local symmetry and multiplicity			
		I		I_h	
Triacontahedron		235		$m\bar{3}5$	
general position	$(x, y, \pm z)$	–	–	1	120
general (*dextro*)	$(x, y, +z)$	1	60	–	–
general (*laevo*)	$(x, y, -z)$	1	60	–	–
in plane m_{38}	$(x, y, 0)$	–	–	m	60
in plane m_{45}	$(x, 0, z)$	–	–	m	60
on 2-fold axis 2_{45}	$(0, 0, 0) \rightarrow (1+\tau, 0, 0)$	2	30	$2mm$	30
on 3-fold axis 3_{348}	$(0, 0, 0) \rightarrow (1, 1+\tau, 0)$	3	20	$3m$	20
on 5-fold axis 5_4	$(0, 0, 0) \rightarrow (1+\tau, \tau, 0)$	5	12	$5m$	12
at origin	$(0, 0, 0)$	235	1	$m\bar{3}5$	1
Rhombic icosahedron		5		$5m$	
general position	(x, y, z)	1	5	1	10
in plane m_{38}	$(x, y, 0)$	–	–	m	5
on 5-fold axis 5_4	$(-1, -1-\tau, 0) \rightarrow (1+\tau, \tau, 0)$	5	1	$5m$	1
Rhombic dodecahedron		2		$2mm$	
general position	(x, y, z)	1	2	1	4
in plane m_{38}	$(x, y, 0)$	–	–	m	2
in plane m_{45}	$(x, 0, z)$	–	–	m	2
on 2-fold axis 2_{45}	$(1-\tau, 0, 0) \rightarrow (1+\tau, 0, 0)$	2	1	$2mm$	1

Table 4 (continued)

Position	Coordinates	Local symmetry and multiplicity			
		I		I_h	
Rhombohedron		3		$3m$	
general position	(x, y, z)	1	3	1	6
in plane m_{38}	$(x, y, 0)$	–	–	m	3
on 3-fold axis 3_{348}	$(1-\tau, -\tau, 0)$ $\rightarrow (1, 1+\tau, 0)$	2	1	$2mm$	1
Faces					
F_1, general position		1	4	m	4
long diagonal		2	2	$2mm$	2
short diagonal		2	2	$2mm$	2
center		222	1	$mm2$	1
F_2, general position		1	2	m	2
long diagonal		2	1	$2mm$	1
F_3, general position		1	2	m	2
short diagonal		2	1	$2mm$	1
Edges					
E_1, general position		5	1	$5m$	1
E_2, general position		5	1	$5m$	1
Vertices					
A, at the center of a star		235	1	$m\overline{3}\overline{5}$	1
B, at the center of a star		235	1	$m\overline{3}\overline{5}$	1
C, at the center of a triacontahedron		235	1	$m\overline{3}\overline{5}$	1

that the cells are nevertheless centrosymmetric. For example, opposite faces of the rhombohedral units are usually treated as similar, even though it is theoretically forbidden. So-called *c*-linkage of Tsai clusters is interpreted in terms of interpenetrating triacontahedra, though triacontahedra never overlap in the Socolar-Steinhard tiling, and so on. Entrenched stereotypes prevent further progress. In general, quasi-unit cells do not coincide in both right-side-up and upside-down orientations. None of the cells has an inversion center for the group I, and therefore so must be the atomic decorations.

Second, the local matching rules appear in the higher-dimensional approach as a natural consequence of the different decorations of faces by the Ammann planes. Our inflation/deflation rules are consistent with the Ammann grid [36], the same must relate to the decorations of faces by atoms. In other words, if we have decorated a single face, then we are obligated to apply the similar decoration scheme to all equivalent faces, regardless of whether they belong to the same cell or to another.

Third, the atomic decoration scheme should not depend on which of three sites (A, B or C) is assigned to the origin of the packing. For example, if the origin is set at the C-type site, there is the only 2-fold axis passing through the face F_1, namely normal to the face. On the other hand, if the origin is set at the B-type site, another 2-fold axis appears, namely passing along its long diagonal. Surely, atomic decorations of faces cannot depend on the coordinate system chosen and should thus be common to all variants due to their local isomorphism. This leads to the conclusion that, when considered locally, the decorated face F_1 should have either 222 or mmm symmetry for the groups I and I_h, respectively. Decorated faces F_2 and F_3 have either 2 or $mm2$ symmetry with principal axes parallel to the long and short diagonals of the rhombuses, respectively.

The inequivalent atomic positions are listed in Table 4. Any single point generates the corresponding full set under the group action. We choose characteristic points in the xy plane or close to the xy plane, whenever possible, to specify the inequivalent positions within the quasi-unit cells. The alternative settings (e.g., in the xz plane or close to z axis) are also possible. Figure 7 will be helpful to better understand the choice of fundamental domains for different quasi-unit cells. Here m_{12} denotes the mirror plane that swaps the vertices 1 and 2. It coincides with the yz plane. The mirror planes m_{38} and m_{45} coincide with the xy and xz

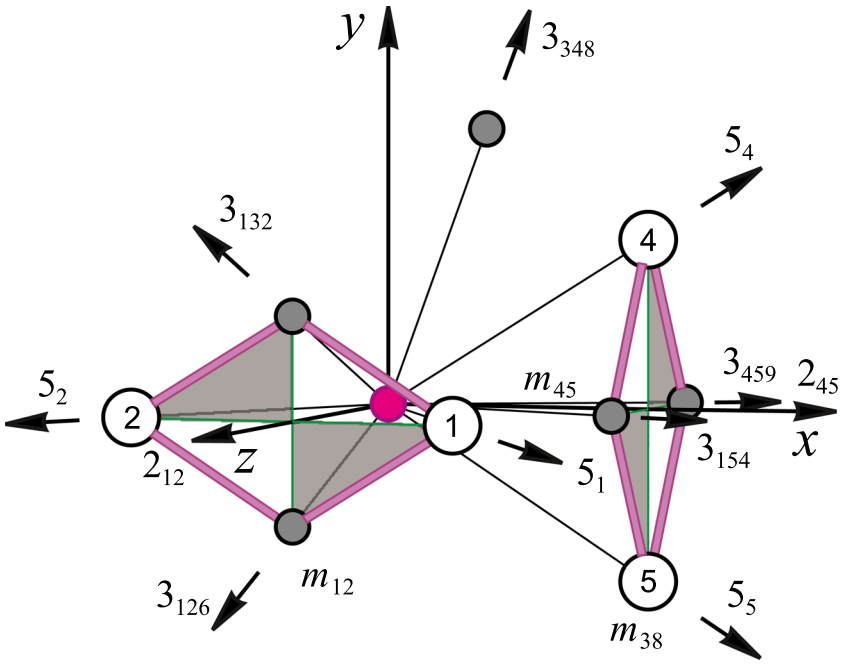

Fig. 7 Possible choices of the fundamental domain in a triacontahedron. For the group I, it might be a region enclosed within a pyramid and bounded by the axes 5_1, 3_{132} and 3_{126}. Two enantiomorphic forms can exist: *dextro*, when an atom in general position falls within the upper part of the domain, and *laevo*, when an atom falls within the lower part. Another possible choice is a region bounded by the axes 5_4, 3_{154} and 3_{459}. For the group I_h, it might be a region bounded by the axes 5_1, 3_{132} and 2_{12}. Another possible choice is a region bounded by the axes 5_4, 3_{154} and 2_{45}

planes, respectively. The 2-fold axis 2_{12} swaps the vertices 1 and 2, too. It coincides with the z axis. The axis 2_{45} coincides with the x axis.

Consider the local symmetry of faces in more detail (Fig. 8). For the group I, a 2-fold axes passes through the center of F_1 as it is the face of a triacontahedron. Another 2-fold axis passes along the long diagonal as it is the face of a rhombohedron, while 20 rhombohedra may be assembled into a star. If two 2-fold axes exist, then a third 2-fold axis appears. The local symmetry of the face F_1 is thus 222. The local symmetry of the faces F_2 and F_3 can be found in a similar way, namely by considering the different choices of the packing origin.

It seems to be incompatible that the local symmetry of triacontahedron faces is higher than just a single 2-fold axis. The multiplicity of general atomic positions on faces is twice as large compared to the positions inside the triacontahedron very close to the surface. How can it be that, when an atom is slowly approaching the surface, its multiplicity suddenly doubles? The simple answer is: when an atom is approaching the surface from inside, another atom is approaching the paired position from outside.

Imagine, for example, a tetrahedrally bounded atom on the surface of a triacontahedron with three bonds directed inward to the cell and one bond directed outward from the surface. Then, there will be a pair of atoms with single bonds directed outwards and another pair of atoms with single bonds directed inwards. For the group I, we mark such positions with open and solid circles, respectively. Note that this difference disappears for the group I_h due to the local mirror plane passing through the face. For the group I_h, the number of equivalent positions close to the surface does not double when the position approaches the face.

Marking of the general positions on cell faces for the group I is shown in Fig. 9. Such marking spots, in fact, provide yet another tool for the formulation of the matching rules (compare with [22]) and must be, therefore, mutually consistent with all the four types of quasi-unit cells. If two quasi-unit cells are placed face-to-face next to each other, then the opposite marking spots must coincide, and furthermore, open circles must coincide with solid circles and vice versa. They may be interpreted as key-lock-pairs. A face with two wide-set spots does not fit the one with two narrow-set spots and also the one with four spots. So,

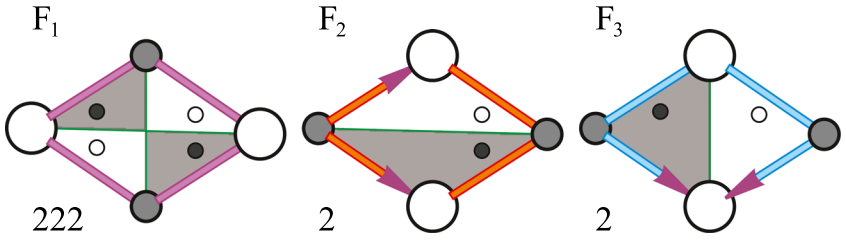

Fig. 8 Local symmetry of faces for the group I

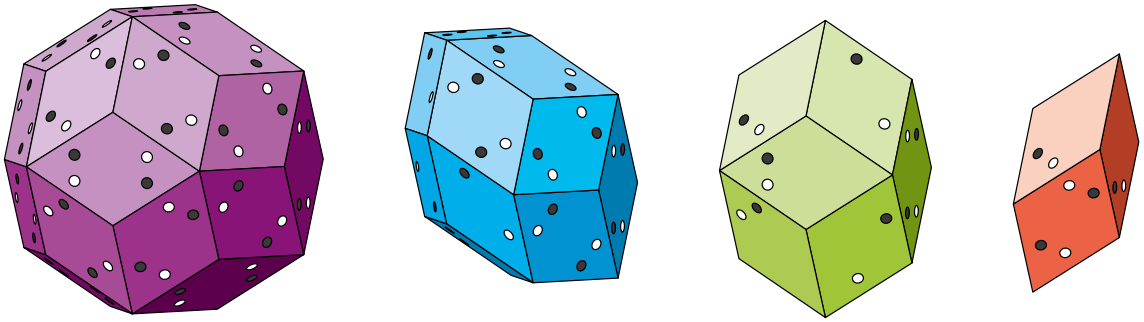

Fig. 9 Marking of the general positions on the cell faces for the group I. The marking spots act as key-lock-pairs when stacking quasi-unit cells face-to-face

when returning to the problem of how to fill the quasi-unit cells with atoms, we emphasize the following: The directed chemical bonds must obey the symmetry rules and we should take into account not only the inequivalent sites themselves but also the local site symmetries when placing the atoms on the faces.

We draw attention to an interesting fact. Consider four atoms in general positions on the faces F_1 and shift them a little inward and outward from the surfaces. If one pair moves inward from the surface, the other moves outward, and vice versa. If we consider each of them in turn, we get an example of two icosahedral enantiomorphs, at least theoretically.

Enumeration of other specific positions seems to be unproblematic. The only complication is the accurate accounting of sharing factors. Positions on the faces are characterized by the sharing factors of 1/2. The sharing factors for atoms on the edges and at the vertices are presented in Fig. 10. This data is necessary for the calculation of chemical composition.

Composition stoichiometry

In order to calculate the packing density and compound stoichiometry, we firstly need to know the relative frequencies of quasi-unit cells, which in turn may be found by applying the Perron projection to the transpose of the substitution matrix [39]:

$$\lim_{k\to\infty}\left(\frac{1}{\tau^9}\mathbf{M}^{\mathrm{T}}\right)^k = \mathbf{v}\otimes\mathbf{w}^{\mathrm{T}}. \tag{3}$$

Here, τ^9 represents the cube of the linear scale factor and is nothing but the Perron-Frobenius eigenvalue, $\mathbf{M}$ is the tiling substitution matrix, while the result of the Perron projection is the Kronecker product of its left and right eigenvectors $\mathbf{v}$ and $\mathbf{w}$, respectively. Recall that every row of the transposed substitution matrix indicates how many quasi-unit cells of the initial size are required to build up the inflated cells, the volume of which becomes τ^9 times greater.

The eigenvectors read:

$$\begin{aligned}\mathbf{v} &= (1,\ 2\tau,\ 5\tau,\ 10\tau)\\ \mathbf{w} &= \frac{1}{10}(6-2\tau,\ -11+7\tau,\ 10-6\tau,\ -3+2\tau)\end{aligned} \tag{4}$$

The components of the vector $\mathbf{v}$ are the relative cell volumes, whereas the components of the vector $\mathbf{w}$ are their absolute appearance frequencies. The vector $\mathbf{w}$ shows how many cells there are per unit volume in the tiling on average. All

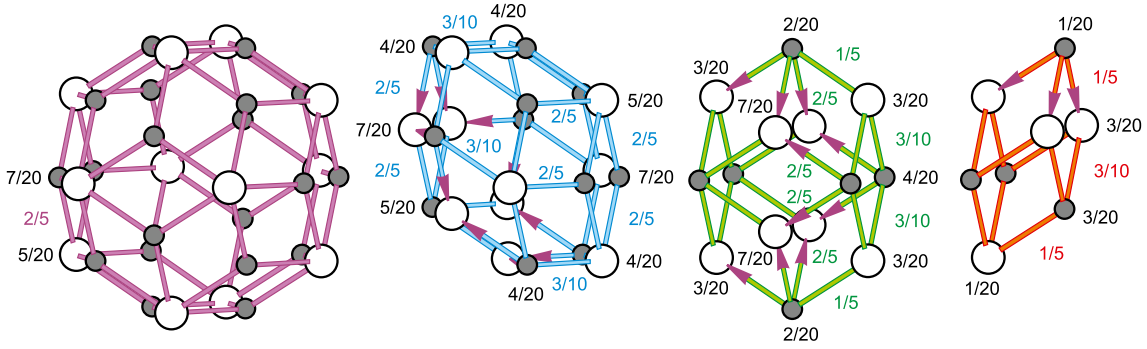

Fig. 10 Sharing factors for atoms on the edges and at the vertices

the frequencies can be expressed through the golden ratio as binomials with rational coefficients.

The simplest way to calculate the vector **w** is to take the substitution matrix and square it several times:

$$\frac{1}{\tau^9}\mathbf{M}^{\mathrm{T}} = \frac{1}{\tau^9}\begin{pmatrix} 21 & 3 & 2\frac{2}{5} & 1\frac{3}{5} \\ 68 & 11 & 6\frac{2}{5} & 5\frac{3}{5} \\ 170 & 20 & 17 & 15 \\ 340 & 30 & 36 & 31 \end{pmatrix} \xrightarrow[\text{by squaring}]{\text{exponentiation}} \ldots \rightarrow \mathbf{v} \otimes \mathbf{w}^{\mathrm{T}} \tag{5}$$

Even after the 3rd squaring the resulting matrix does not change much anymore. The 4th iteration corresponds to the $2^4 = 16$ consecutive inflations so that the averaging occurs over the region with linear dimensions $\sim 10^{10}$ times as large as the initial cell size. The 4th iteration guarantees that the averaging region is macroscopic in size. The first row of the obtained matrix provides the required occurrence frequencies.

If an atom occupies a certain position (see Table 4), we need to calculate the occupancy vector **p** taking into account all equivalent sites. Four components of the vector **p** are the numbers of specific atoms in the cells of each type, respectively. We need to multiply the corresponding multiplicity and sharing factors and sum the products over the cells taking into consideration the numbers of faces, edges, and vertices if necessary. For example, if certain atoms occupy the vertices A, the occupancy vector is given by $\mathbf{p} = (\frac{1}{2}, 2, 3, 3)$. If, conversely, the vertices B are occupied, $\mathbf{p} = (\frac{1}{2}, 1, 3, 7)$. Well, all that remains is to take the dot product:

$$d = (\mathbf{p} \cdot \mathbf{w}) \tag{6}$$

The value of d shows how many atoms of a given sort exist per unit volume, when the volume of an elementary rhombohedron is assumed to be 1.

To calculate the X-ray density, we have merely to execute the similar procedure for all the occupied positions and for all sorts of atoms. Another interesting observation is that stoichiometric coefficients can always be expressed through the golden mean. The composition of conventional periodic crystals is given by the ratio of two or more integers. The stoichiometric composition of icosahedral quasicrystals is given by the ratio of algebraic integers, namely belonging to the ring of quadratic integers $\mathbb{Z}\left[\frac{1+\sqrt{5}}{2}\right] = a + b\tau$ of the field $\mathbb{Q}(\sqrt{5})$ [52]. In other words, their composition can always be expressed through the binomials of τ with integer coefficients.

Of course, this relates to the exact stoichiometric composition of perfect quasicrystals. Intermetallic compounds usually have wide homogeneity regions in phase diagrams. Icosahedral quasicrystals are no exception and can also exhibit the deviations from stoichiometry like any other chemical compounds of variable composition (berthollides).

Diffraction pattern

Diffraction patterns of icosahedral quasicrystals are characterized by the sets of aperiodically arranged sharp diffraction peaks (Bragg peaks). Our goal is to provide a tool, which enables the calculation of structure factors without leaving the real physical space. When considering diffraction of plane waves within the kinematic theory of scattering, we have to deal with similar terms in the form of $f_j \exp[i(\mathbf{k}\mathbf{r}_j)]$, where $\mathbf{r}_j$ and $\mathbf{k}$ represent the vectors in direct and reciprocal space, respectively, and f_j are the atomic scattering factors. Scattering by rotated quasi-unit cells can be described by terms $f_j \exp[i(\mathbf{k}\hat{g}\mathbf{r}_j)]$. The symmetry transformation g is considered here as an operator. The action of the group element can be interpreted either as the left-action on the real vector, or as the right-action on the reciprocal vector. The first approach forces us to consider all the differently oriented cells as independent ones so that the total number of cells becomes as large as 63 (see Fig. 3). The second approach does not lead to an increase in the number of cells but entangles the reflexes with equivalent sets of Miller indices. We have opted for the increased basic set.

The calculation procedure is as follows. Suppose we have chosen an appropriate decoration scheme for all cells. At the first step, for a given scattering vector **k**, we calculate the partial structure factors F_k for every quasi-unit cell bearing in mind the difference between the rotated cells:

$$F_k = \sum_j f_j \exp[i(\mathbf{k}\mathbf{r}_j)] \tag{7}$$

Here, f_j and $\mathbf{r}_j$ are the atomic scattering factor and the position of the jth atom in the kth cell. The atomic coordinates are given with respect to the local coordinate systems. Rotation of cells occurs about their local origins. Atomic scattering factors should be multiplied by sharing factors when necessary.

Let us temporarily denote the initial structure factors as $F_k^{(0)}$. Then, inflate and deflate the cells and consider their partial structure factors $F_k^{(1)}$ again. Continue the inflations and deflations up to infinity. Every time, the linear cell dimensions become τ^3 times larger, whereas the cell volumes become τ^9 times larger. The atomic form factor is defined as the Fourier transform of the scattering density. The structure factor of a single cell is, in turn, the Fourier transform of the scattering density and splits into the sum of atomic form factors multiplied by corresponding phase

factors. The structure factor of an inflated supercell is, in turn, the Fourier transform and splits into the sum of the structure factors of subcells multiplied by corresponding phase factors, and so forth:

$$\begin{aligned} F_k^{(0)} &= \sum_j f_j \exp[i(\mathbf{k}\mathbf{r}_j)] \\ F_k^{(1)} &= \sum_j F_j^{(0)} \exp[i(\mathbf{k}\mathbf{R}_j)] \\ F_k^{(2)} &= \sum_j F_j^{(1)} \exp[i(\mathbf{k}\cdot\tau^3\mathbf{R}_j)] \\ &\dots \\ F_k^{(n+1)} &= \sum_j F_j^{(n)} \exp[i(\mathbf{k}\cdot\tau^{3n}\mathbf{R}_j)] \end{aligned} \tag{8}$$

Here, $\mathbf{R}_j$ is the position of the jth subcell in the decomposition of the kth supercell. The partial structure factors of initial cells play the role of atomic scattering factors in corresponding equations as if the quasi-unit cells were "composite" atoms which comprise the supercells.

We see that the partial structure factors of the inflated quasi-unit cells are represented by the linear combinations of the initial ones. Therefore, we can write this set of linear equations in the matrix form.

We define a special matrix $\mathbf{S}$ which we can refer to as the scattering substitution matrix [39]. If a specific cell in a specific orientation appears in the decomposition, the respective phase factor appears at the intersection of the corresponding row and column. Of course, the phase factors should be multiplied by the sharing factors for the shared subcells. We emphasize that the differently oriented quasi-unit cells should be counted as separate ones at this stage. The matrix $\mathbf{S}$ is thus a 63×63 matrix. We go through all entries of the array of rules and fill the entries of the matrix $\mathbf{S}$ by corresponding sums of the products of the phase and sharing factors.

The kinematic theory of scattering neglects the multiple diffraction effects. We have thus reasons to expect that the following procedure results in the required (complex) weighting factors for the averaging of partial structure factors:

$$\mathbf{F}^{(n+1)} = \mathbf{S}^{(n)} \cdot \dots \cdot \mathbf{S}^{(1)}\mathbf{S}^{(0)}\mathbf{F}^{(0)} = \left(\prod_{k=0}^{n} \mathbf{S}^{(k)}\right)\mathbf{F}^{(0)} \tag{9}$$

Each inflation is accompanied by a volume increase. On the other hand, the intensity of the diffracted beam is proportional to the volume of the irradiated homogeneous medium. Therefore, to normalize the intensities to the volume of an initial rhombohedron, we should divide each matrix $\mathbf{S}^{(k)}$ by a factor of τ^9, write down a respective sequence of matrix products, and then find its limit:

$$\dots \cdot \frac{\mathbf{S}^{(n)}}{\tau^9} \cdot \dots \cdot \frac{\mathbf{S}^{(1)}}{\tau^9} \cdot \frac{\mathbf{S}^{(0)}}{\tau^9} = \prod_{k=0}^{\infty} \frac{\mathbf{S}^{(k)}}{\tau^9} \tag{10}$$

This sequence converges very fast. Even the 6th inflation corresponds to the micrometer-sized grains so that about five consecutive matrix multiplications ensure averaging of the coherently scattered waves over several millions of quasi-unit cells.

Strictly speaking, this procedure is not the Perron projection, though it is very similar to it. The matrices $\mathbf{S}^{(k)}$ differ from each other due to the factors of τ^3 (see Eq. 8). Their entries are complex, not real. We expect that the dominating eigenvalues of all matrices $\mathbf{S}^{(k)}$ are equal to τ^9, but we cannot prove it. We also cannot prove that the matrix sequence necessarily converges with $n \to \infty$, and namely to the degenerate matrix all rows of which differ from each other by constant (complex) factors only. At the moment, we shall confine ourselves to saying only that further investigations are needed.

If we do not focus on the pure mathematical aspects, we can conclude that, finally, the computation of the average structure factors splits into the following steps: First, we calculate the column vector, which entries are the partial structure factors, whereby the differently oriented quasi-unit cells should be counted as different ones. Then, we compute the scattering substitution matrices and create the special matrix sequence as described above. Next, we find the limit of that sequence and write down the first row from the resulting matrix. It contains the required complex weighting factors. Finally, we take the dot product of both vectors to obtain the average structure factor for the Bragg peak under consideration.

Characteristic clusters and their spatial arrangement

Conventional approaches to solve the Patterson map immediately in higher dimensions may not always be appropriate for interpretation of atomic positions in real space within the standard cut-and-project procedure. Indeed, when describing the generation of the Fibonacci chain by strip projection, Steurer and Haibach [53] write the following: "The physical space $\mathbf{V}^{\parallel}$ is related to the eigenspace of the substitution matrix S associated with its eigenvalue $\lambda_1 = \tau$. The perpendicular space $\mathbf{V}^{\perp}$ corresponds to the eigenspace of the substitution matrix S associated with its eigenvalue $\lambda_2 = -1/\tau$. Thus, the physical space scales to powers of τ and the perpendicular space to powers of $-1/\tau$." The further apart are two

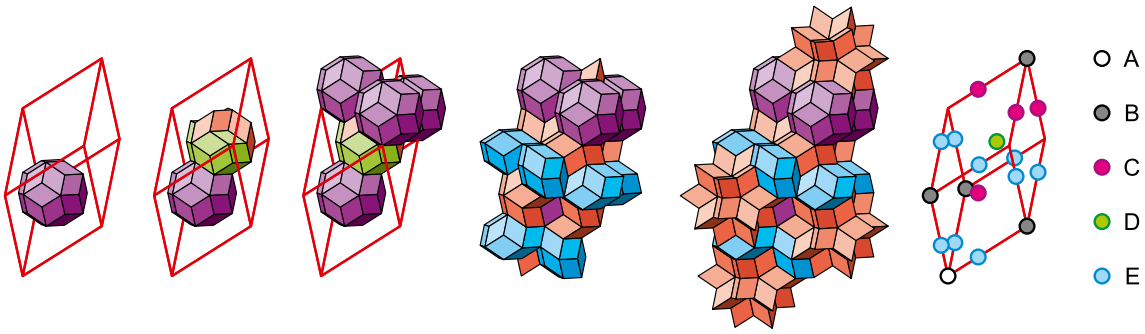

Fig. 11 An example of the cell decoration scheme. (A) The centers of A-stars, (B) the centers of B-stars, (C) the centers of triacontahedra, (D) positions on the diagonals of such rhombohedra which are surrounded by three rhombic dodecahedra, and (E) positions on the 5-fold axes of rhombic icosahahedra

equivalent points in physical space after inflations, the closer are the corresponding points in perpendicular space. In particular, this means that those closely spaced peaks on the Patterson map, which are usually interpreted as unreasonable in physical space in comparison with the shortest interatomic distances, may be allowed in perpendicular space $\mathbf{V}^{\perp}$. This has prompted us to search for uniform and simple rules to fill the quasi-unit cells with atoms without appealing to higher dimensions.

Figure 11 shows such an example. We consider the Socolar-Steinhardt tiling and suppose that the cells are filled as follows. Some atoms, say of the type A, occupy the centers of the complete A-stars. Similarly, atoms B occupy the centers of the B-stars. Atoms C occupy the centers of triacontahedra. Further, we search over the entire tiling for special clusters of four rhombohedra and three rhombic dodecahedra. Such clusters together with neighboring triacontahedra were usually interpreted as *c*-linkage of overlapping triacontahedra up to now. We place the atoms D inside each of such clusters somewhere on the long diagonal of the central rhombohedron. Next, we place the atoms E somewhere on the 5-fold axes of initial rhombic icosahedra. Note that rhombic icosahedra generate equivalent positions on the edges E_1 of inflated cells. Finally, we apply the similar decoration scheme to all the four types of quasi-unit cells (Fig. 12). The special features of the as-obtained packing are as follows.

The Tsai cluster appears from the triacontahedron as a result of the cell decoration. It consists of four consecutive shells: the dodecahedron, the icosidodecahedron, the icosahedron and the outer thiacontahedron with additional atoms on its edges. The Tsai cluster is centered with a C-type atom. The 2nd shell is built of C-type atoms too and has the fixed size. The relative size of the 1st and the 3rd shells may vary. The smaller the 3rd (icosahedral) shell is, the closer the corresponding atoms in the last (triacontahedral) shell to the mid-points of the edges are and also to the B-type vertices. If we choose the position of the E-type atom so that it coincides with the local origin of the rhombic icosahedron, the 2nd and 3rd shells join into an icosahedron with triangulated faces. Such packing geometry is characteristic of the Mackay cluster.

All cells inherit the decoration scheme of the Tsai cluster. A half of the Tsai cluster appears inside the rhombic icosahedron. A smaller wedge slice predefines the decoration of the rhombic dodecahedron. A very small triangle piece of the Tsai cluster predefines the decoration of the rhombohedron (Fig. 12). Distribution of atoms within the three of four cells is strongly non-centrosymmetric.

There are no pairs of interpenetrating triacontahedra in our model, because the second of them is, in fact, a composite sphere-like cluster of seven subcells with integral 3-fold symmetry (see Fig. 11). Such assumption predetermines the asymmetric positioning of triacontahedra within the inflated rhombohedron: one triacontahedron is situated at the local cell origin on the long diagonal, whereas the other three triacontahedra are situated on the edges on the opposite side. Such type of mutual arrangement of triacontahedra in icosahedral quasicrystals has been reported earlier by Audier et al. [54].

No disordered tetrahedra exist inside the Tsai clusters. Moreover, what we mean is that such tetrahedra appear due to the erroneous identification of sphere-like 3-fold clusters, when such clusters are wrongly equated with interpenetrating triacontahedra and forcibly fitted to higher symmetry.

Some of the A-type vertices of the Tsai clusters are not occupied. Return to Fig. 4. We suggested that only those of the A-type vertices are occupied that are the centers of stars. However, some vertices do not transform into complete A-stars after the first deflation, namely those of them to which the arrows point, irrespective of whether the arrows denote the E_2 edges of the cell under consideration or the arrows point to the cell vertices from outside. Such vertices should be thus unoccupied. This ambiguity can be removed after two consecutive inflations and deflations.

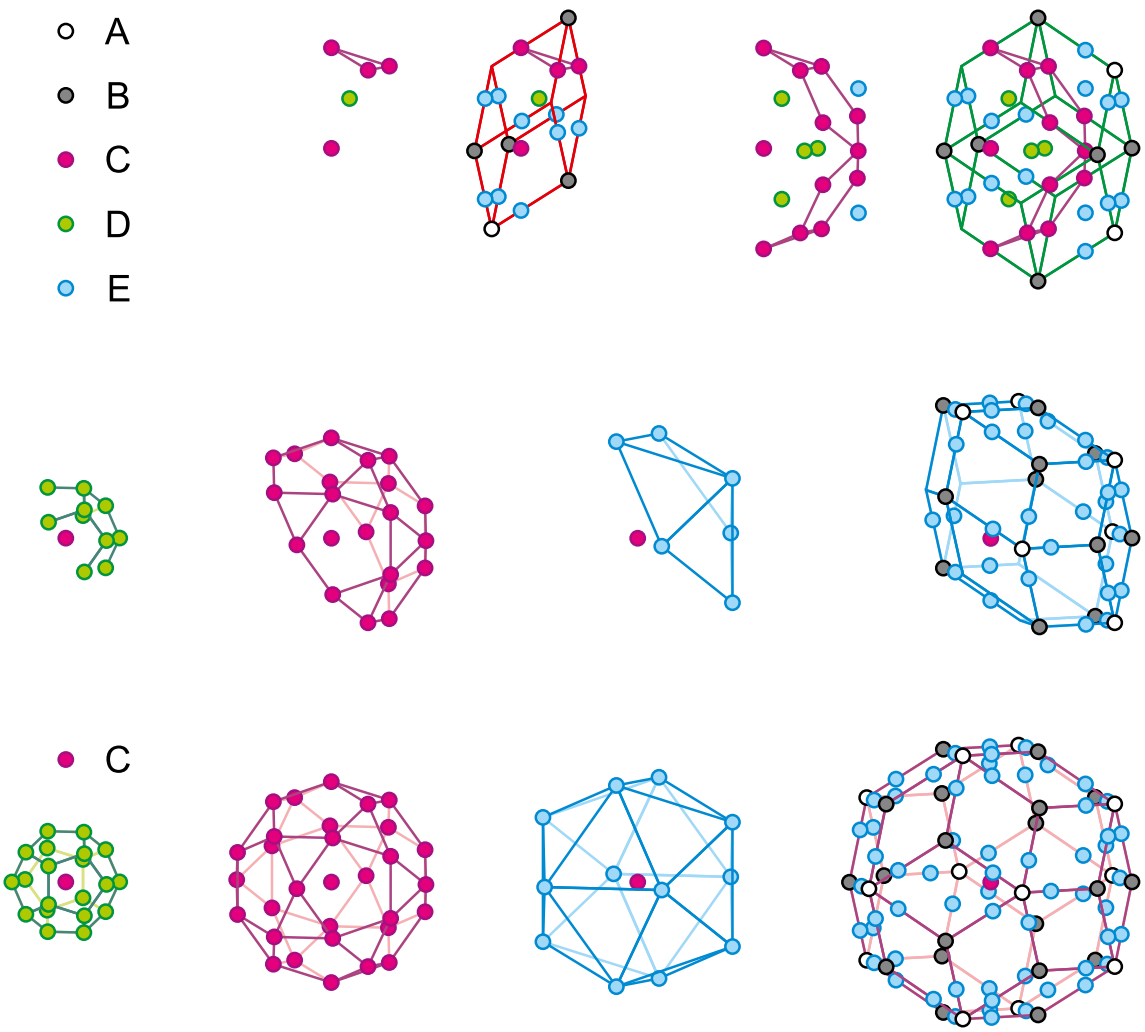

Fig. 12 Decoration of quasi-unit cells. As a result, the Tsai cluster appears from the triacontahedron. Other cells inherit the decoration scheme of the Tsai cluster

Now we set the origin of the global coordinate system at the A- and B-type sites, respectively, and apply the similar decoration scheme. As a result, we obtain the remaining two locally isomorphic packings and two additional families of multi-shell icosahedral clusters (Fig. 13). Any of them appears infinitely many times in the packing alongside with the Tsai clusters.

The sequence of shells and their relative size almost completely reproduce the structure of characteristic clusters found in Al-Pd-Mn quasicrystals [11]. Moreover, we have an interesting observation: if the C-type sites are occupied by the Tsai clusters, then the A-type sites are occupied by the Bergman clusters.

Recall that we introduced only two variable parameters: the position of the atom D on the 3-fold axis and the position of the atom E on the 5-fold axis. The relative shell size of any shell in any cluster is either determined by one of these parameters or fixed. We see that the structures of characteristic clusters reproduce "in general" the main structural motifs of known icosahedral quasicrystals and their approximants [10, 11, 51, 55–58], especially when bearing in mind that some of the shells can swap.

The next interesting feature is the spatial arrangement of the Tsai clusters (Fig. 14). They can form icosahedra, dodecahedra and icosidodecahedra when stacked face-to-face. A dodecahedral hierarchical shell of Tsai clusters surrounds the A-type site. An icosahedron, whose vertices are occupied by the Tsai clusters, surrounds the B-type site. A fascinating hierarchical cluster of clusters appears around the C-type site. The central Tsai cluster, which is represented by a single point in Fig. 14, is surrounded by an icosidodecahedron, whose vertices are occupied by the Tsai clusters. In turn, it is surrounded by a hierarchical cluster of clusters—icosidodecahedron, whose vertices are occupied by icosidodecahedra, whose vertices are occupied by the Tsai clusters. Positions of the Tsai clusters between a central icosidodecahedron and the ring of icosidodecahedra are strongly ordered and inherit the decoration scheme of

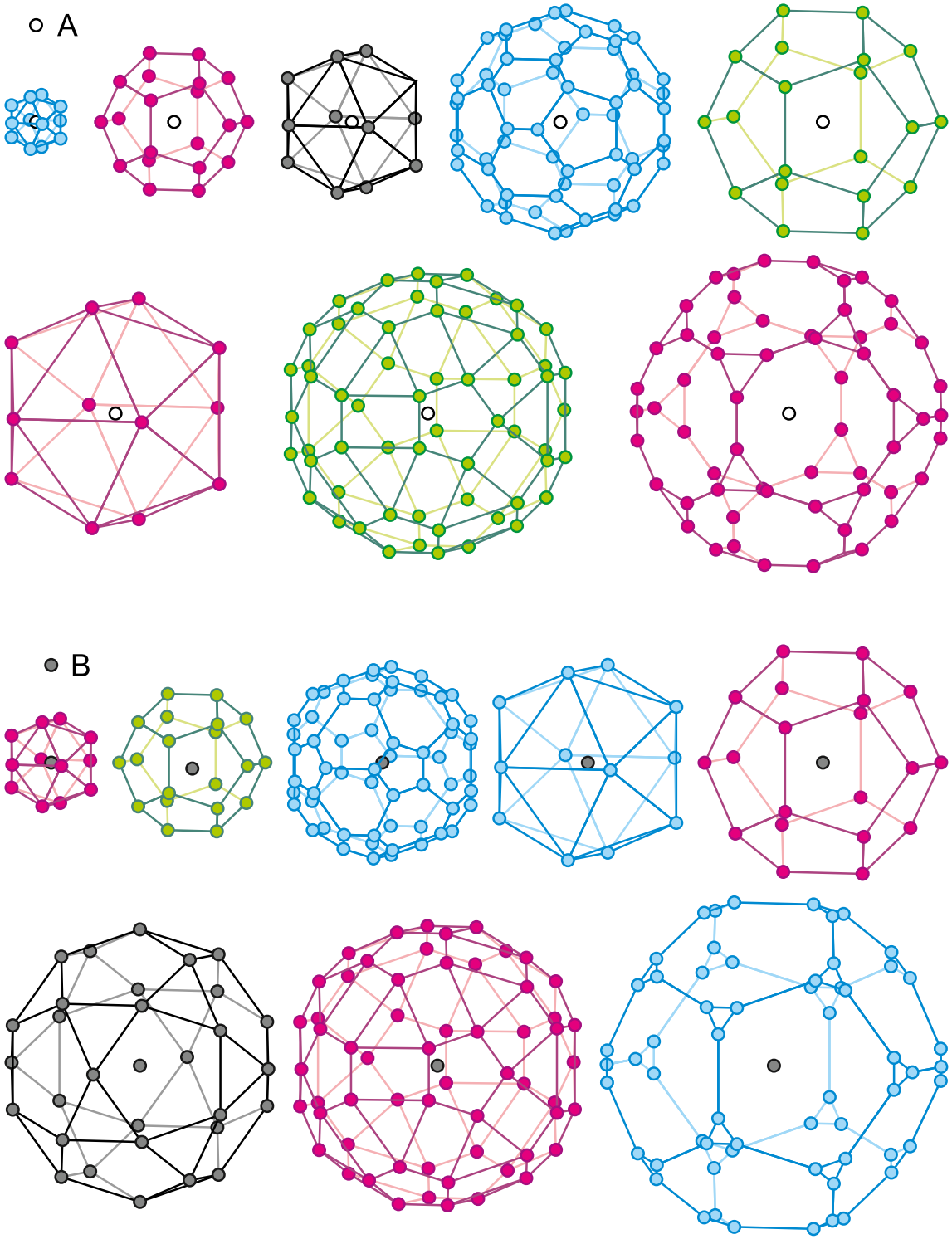

Fig. 13 Multi-shell structure of characteristic clusters centered at the sites A and B in the case when the C-type sites are occupied by the Tsai clusters

rhombic dodecahedra (see the remarkable wedge slices in Fig. 12). In projection along the 5-fold axis, the clusters form characteristic patterns of decagons and pentagons.

This picture almost exactly reproduces the main structural motif of the Yb-Cd family of icosahedral quasicrystals [12, 14]. The key differences are the following: (i) The spatial arrangement of the Tsai clusters actually lacks the 5-fold symmetry in a standard model especially in the region between the central icosidodecahedron and the ring of icosidodecahedra. Our model does not have this disadvantage

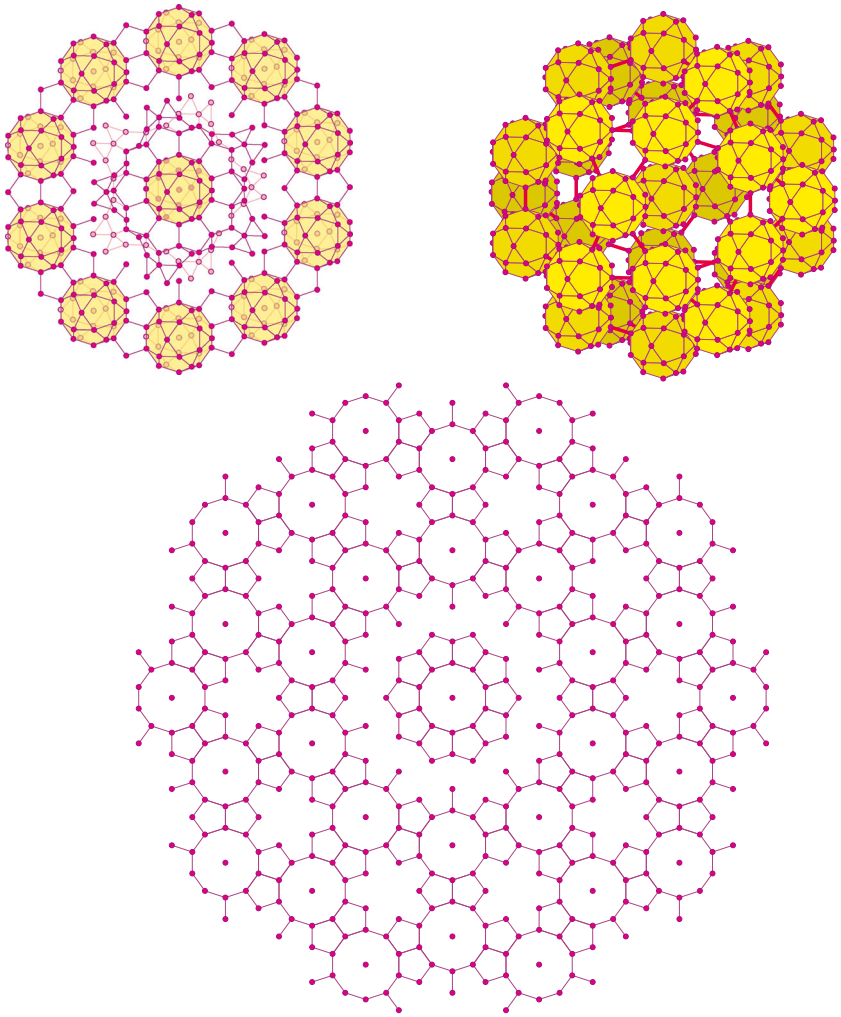

Fig. 14 Spatial arrangement of Tsai clusters. They form self-similar hierarchical clusters of clusters: icosidodecahedra, whose vertices are occupied by icosidodecahedra, whose vertices are occupied by the Tsai clusters. In projection along the 5-fold axis, they form characteristic patterns of decagons and pentagons

(compare with a dense plane of triacontahedral units projected along the 5-fold axis, see Fig. 5 in [12]). (ii) The innermost disordered tetrahedral units inside the triacontahedron do not appear in our model. On the contrary, a C-type atom appears at the center of the cluster. (iii) In the commonly accepted model, the icosahedral shell is assumed to be occupied by the ytterbium atoms, whereas the mid-edges of the triacontahedron are occupied by cadmium. In contrast, both positions are interrelated in our model, so that we expect that they should be occupied by similar atoms. (iv) There are a lot of partially occupied positions in a standard model, as well as positions with mixed occupancies, because a substitutional disorder in atomic occupation is an intrinsic property of such chemical compounds. (v) Hundreds of variable parameters are usually needed in practical refinements [14]. Only two parameters define the relative atomic positions in our model.

What we mean to say is that "the truth is somewhere in between".

Results and discussion

The multiple-cell approach includes the group-theoretical analysis of the packing symmetry, selection of an appropriate set of quasi-unit cells, formulation of the substitution rules, formulation of the space-filling algorithm, enumeration of inequivalent atomic positions in quasi-unit cells and formulation of corresponding decoration rules, selection of an appropriate cell decoration scheme and, finally, the construction of the packing with subsequent analysis of substitution matrices both in real and reciprocal space. The similar approach can be applied to almost all types of quasicrystals (see, e.g., [59]). For example, if the Penrose tiling is laid down on the basis of the packing, two right prisms with rhombic bases may be used as quasi-unit cells. We hope that such approach could give a new insight into the general problem of aperiodicity [60–62].

Both I and I_h symmetry groups can be considered within the multiple-cell approach; meanwhile, both left-handed

and right-handed enantiomorphic forms can be resolved for the group I at the stage of cell decoration. For example, we can imagine a hierarchically built skewed icosahedron (see, e.g., a geometric model of the papilloma viral capsid [63]) and put it inside the largest quasi-unit cell, a half of it—inside the smaller cell, a wedged slice—inside the even smaller one, and a small triangle piece put inside the rhombohedron, so that such procedure results in a non-centrosymmetric quasicrystalline packing of viral capsomers.

The next interesting question is the shape of the Brillouin zone. This problem has been extensively treated by both theoretical and experimental methods. In particular, selected area diffraction from artificial aperiodic structures has been used for the Brillouin zone visualization. Toroidal topology of fundamental domains has been widely discussed in this regard [64–67]. On the other hand, icosahedral quasicrystals obey the icosahedral symmetry both in real and reciprocal space. In the same manner as four quasi-unit cells fill the real space, the four Brillouin subzones can fill the reciprocal space. Recall that the Brillouin zone contains all irreducible representations, which are indexed with a wave vector **k**. It may not necessarily be a single bounded set.

The calculation technique based on the scattering substitution matrices can provide the researchers with the effective tool for the description of scattering phenomena and manipulation of optical fields in deterministic aperiodic nanostructures [68], as well as facilitate further progress in the field of photonic quasicrystals [69, 70]. Another possible area of application lies in the architectural acoustics, particularly in designing the sound shielding and acoustic ceiling systems [71].

Conclusion

The multiple-cell approach is proposed as an alternative to the higher-dimensional crystallographic description of icosahedral quasicrystals. Four types of golden zonohedra serve as quasi-unit cells. They fill the space without gaps and overlappings. Every quasi-unit cell is decorated by specific atoms and associated with a triad: type, position, and orientation. Both I and I_h symmetry groups can be distinguished at the stage of cell decoration. Both the Tsai and the Bergman clusters appear as a result of a simple five-component decoration scheme. The mutual arrangement of characteristic clusters is in a good agreement with the known icosahedral structures.

Acknowledgments We thank Jelena R. Kambak for proofreading and writing assistance.

Funding information This work is partially supported by the Ministry of Education and Science of the Russian Federation, Grant 16.8549.2017/8.9.

Compliance with ethical standards

Conflict of interest The authors declare that they have no conflict of interest.

References

1. Shechtman D, Blech I, Gratias D, Cahn JW (1984) Phys Rev Lett 53:70
2. Mackay AL (1982) Physica A 114(1):609
3. Levine D, Steinhardt PJ (1986) Phys Rev B 34:596
4. Socolar JES, Steinhardt PJ (1986) Phys Rev B 34:617
5. Kramer P, Neri R (1984) Acta Cryst A 40(5):580
6. Steurer W, Deloudi S (2009) Crystallography of quasicrystals. Concepts, methods and structures. Springer, Berlin
7. Steurer W (2011) Angew Chem Int Ed 50(46):10775
8. Quiquandon M, Gratias D (2006) Phys Rev B 74:214205
9. Quiquandon M, Gratias D (2014) C R Phys 15(1):18
10. Quiquandon M, Portier R, Gratias D (2014) Acta Cryst A 70(3):229
11. Yamamoto A, Takakura H, Tsai AP (2003) Phys Rev B 68:094201
12. Takakura H, Gómez CP, Yamamoto A, de Boissieu M, Tsai AP (2007) Nature Mater 6(12):58
13. Yamada T, Takakura H, Euchner H, Gómez CP, Bosak A, Fertey P, de Boissieu M (2016) IUCrJ 3(4):247
14. Yamada T, Takakura H, de Boissieu M, Tsai AP (2017) Acta Cryst B 73(6):1125
15. Pham J, Meng F, Lynn MJ, Ma T, Kreyssig A, Kramer MJ, Goldman AI, Miller GJ (2018) J Am Chem Soc 140(4):1337
16. Steinhardt PJ, Jeong HC, Saitoh K, Tanaka M, Abe E, Tsai AP (1998) Nature 396:55
17. Jeong HC, Steinhardt PJ (2003) Phys Rev B 68:064102
18. Mihalkovič M, Zhu WJ, Henley CL, Oxborrow M (1996) Phys Rev B 53:9002
19. Mihalkovič M, Zhu WJ, Henley CL, Phillips RB (1996) Phys Rev B 53:9021
20. Mihalkovič M, Widom M (2006) Philos Mag 86(3–5):519
21. Kato K, Ninomiya T (2002) J Alloy Compd 342(1):206
22. Hann CT, Socolar JES, Steinhardt PJ (2016) Phys Rev B 94:014113
23. Abe E, Yan Y, Pennycook SJ (2004) Nature Mater 3(11):759
24. Tsai AP (2008) Sci Technol Adv Mater 9(1):013008
25. Fujita N, Takano H, Yamamoto A, Tsai AP (2013) Acta Cryst A 69(3):322
26. Lin Q, Corbett JD (2010) Inorg Chem 49(22):10436
27. Guyot P, Audier M (2014) C R Phys 15(1):12
28. Goldman AI, Kelton KF (1993) Rev Mod Phys 65:213
29. Dmitrienko VE, Chizhikov VA (2006) Crystallogr Rep 51(4):552
30. Lidin S (2017) In: Dronskowski R, Kikkawa S, Stein A (eds) Handbook of solid state chemistry, vol 1. Wiley-VCH, pp 73–92. chap. 2
31. Pankova AA, Akhmetshina TG, Blatov VA, Proserpio DM (2015) Inorg Chem 54(13):6616
32. Steurer W (2018) Acta Cryst A 74(1):1
33. Hargittai I (2007) Srtuct Chem 18(5):533
34. Hargittai I (2011) Isr J Chem 51(11–12):1144
35. Gratias D, Quiquandon M (2019) C R Phys 20(7-8):816
36. Madison AE (2015) Struct Chem 26(4):923
37. Madison AE (2015) RSC Adv 5:5745
38. Madison AE (2015) RSC Adv 5:79279
39. Madison AE, Madison PA (2019) Proc Roy Soc A 475:20180667
40. Kramer P, Haase RW (1989) In: Jarić MV (ed) Aperiodicity and order, vol 2. Academic Press, San Diego, pp 81–146. chap. 3

41. Litvin DB (1991) Acta Cryst A 47(2):70
42. Martinez-Torres E, Lopez-Gonzalez JJ, Fernandez-Gomez M, Cardenete-Espinosa A (1989) J Chem Educ 66(9):706
43. Hu WM, Yong JL, Zhou J, Shu F (1987) Superlattices Microstruct 3(4):391
44. Shirai K (1992) J Phys Soc Jpn 61(8):2735
45. Natarajan P, Lander GC, Shepherd CM, Reddy VS, Brooks CL III, Johnson JE (2005) Nat Rev Microbiol 3(10):809
46. Carrillo-Tripp M, Shepherd CM, Borelli IA, Venkataraman S, Lander G, Natarajan P, Johnson JE, Brooks CL III, Reddy VS (2009) Nucleic Acids Res 37(suppl_1):D436
47. Dresselhaus MS, Dresselhaus G, Jorio A (2008) Group theory: Application to the physics of condensed matter. Springer, Berlin
48. Ogawa T (1985) Phys Soc Jpn 54(9):3205
49. Danzer L (1989) Discrete Math 76(1):1
50. Baake M, Grimm U (2013) Aperiodic order, vol 1. Cambridge University Press, Cambridge
51. Steurer W, Deloudi S (2008) Acta Cryst A 64(1):1
52. Levitov LS (1988) EPL 6(6):517
53. Steurer W, Haibach T (2006) In: Shmueli U. (ed) International tables for crystallography Volume B: Reciprocal space. Springer, Dordrecht, pp 486–532
54. Audier M, Sainfort P, Dubost B (1986) Philos Mag B 54(4):L105
55. Audier M, Pannetier J, Leblanc M, Janot C, Lang JM, Dubost B (1988) Physica B 153(1):136
56. Sugiyama K, Kaji N, Hiraga K, Ishimasa T (1998) Z Kristallogr 213(2):90
57. Lin Q, Corbett JD (2006) Proc Natl Acad Sci USA 103(37):13589
58. Akhmetshina TG, Blatov VA (2017) Struct Chem 28(1):133
59. Steurer W (2004) Z Kristallogr 219(7):391
60. Bolotina NB (2007) Crystallogr Rep 52(4):647
61. Janssen T, Janner A (2014) Acta Cryst A 70(4):617
62. Grimm U (2015) Acta Cryst B 71(3):258
63. Shevchenko VY, Madison AE, Mackay AL (2007) Struct Chem 18(3):343
64. Man W, Megens M, Steinhardt PJ, Chaikin PM (2005) Nature 436(7053):993
65. Peach M (2006) Mater Today 9(7):1369
66. Gambaudo JM, Vignolo P (2014) New J Phys 16(4):043013
67. Rosenfeld VR (2017) J Math Chem 55(10):1941
68. Dal Negro L, Lawrence N, Trevino J, Walsh G (2014) In: Dal Negro L. (ed) Optics of aperiodic structures: Fundamentals and device applications. Pan Stanford Publishing, New York, pp 1–56. chap. 1
69. Poddubny AN, Ivchenko EL (2010) Phys E 42(7):1871
70. Vardeny ZV, Nahata A, Agrawal A (2013) Nat Photonics 7(3):177
71. Ajlouni R (2018) ENQ/Enquiry ARCC J Archit Res 15(1):42